Microwave Detection Using Two-Atom-Thick Self-Switching Diodes Based on Quantum Simulations and Advanced Circuit Models

M. Aldrigo, *Member, IEEE*, M. Dragoman, N. Pelagalli, E. Laudadio, L. Zappelli, *Member, IEEE*, S. Iordanescu, *Life Member, IEEE*, D. Vasilache, A. Dinescu, L. Pierantoni, *Senior Member, IEEE*, P. Stipa, and D. Mencarelli, *Member, IEEE*

***Abstract*— In this article, a two-atom-thick diode based on 2-D materials is presented for microwave detection. The diode consists of a molybdenum disulfide monolayer/graphene monolayer heterojunction transferred onto a silicon/silicon dioxide substrate and patterned by means of nanolithography techniques to obtain a geometrical self-switching diode. The interaction between the two monolayers gives rise to a double-stage device, which behaves as a back-to-back diode in the [−3, +3] V voltage range, and as a tunnel diode when exceeding +10 V. The heterojunction can be reproduced at the wafer scale, thanks to its CMOS compatibility and ease of fabrication, and it can be used efficiently as a microwave detector up to 10 GHz, with the best performance around the ISM 2.45-GHz band. Starting from advanced quantum simulations to predict the dc behavior of the single heterojunction-based channel, the diode was fabricated and fully characterized experimentally. Lastly, a rigorous equivalent circuit model is provided, which relies on the measured scattering parameters at high frequencies and allows treating the diode embedded into a coplanar waveguide line as a two-port lossy device. This way, the device can be exploited in circuit-based numerical tools for the design of complex microwave front ends.**

***Index Terms*— Design of microwave devices and circuits, diodes, equivalent circuits, graphene, heterojunctions, modeling, molybdenum disulfide, nanotechnology.**

Manuscript received July 22, 2021; revised October 19, 2021; accepted October 30, 2021. Date of publication December 3, 2021; date of current version February 7, 2022. This work was supported in part by the European Project H2020 NANO-EH under Grant 951761, in part by the two grants of the Romanian Ministry of Research, Innovation and Digitalization, CCCDI—UEFISCDI: under Project PN-III-P3-3.6-H2020-2020-0072 and Project PN-III-P4-ID-PCCF-2016-0033, within PNCDI III, and in part by CINECA-HPC ISCRA MARCONI-100 Computer System under Project n. HP10CMPMGP. This paper is an expanded version from the 2021 IEEE MTT-S International Microwave Symposium (IMS2021), Atlanta, GA, USA; In-Person Event: June 7–10, 2021, Virtual Event: June 20–25, 2021 [DOI: 10.1109/IMS19712.2021.9574815]. *(Corresponding author: M. Aldrigo.)*

M. Aldrigo, M. Dragoman, S. Iordanescu, D. Vasilache, and A. Dinescu are with the National Institute for Research and Development in Microtechnologies, IMT-Bucharest, 077190 Voluntari, Romania (e-mail: martino.aldrigo@imt.ro; mircea.dragoman@imt.ro; sergiu.iordanescu@imt.ro; dan.vasilache@imt.ro; adrian.dinescu@imt.ro).

N. Pelagalli, L. Zappelli, L. Pierantoni, P. Stipa, and D. Mencarelli are with the Department of Information Engineering, Università Politecnica delle Marche, 60131 Ancona, Italy (e-mail: n.pelagalli@pm.univpm.it; l.zappelli@staff.univpm.it; l.pierantoni@staff.univpm.it; d.mencarelli@staff.univpm.it).

E. Laudadio and P. Stipa are with the Department of Materials, Environmental Sciences and Urban Planning, Università Politecnica delle Marche, 60131 Ancona, Italy (e-mail: e.laudadio@staff.univpm.it; p.stipa@staff.univpm.it).

Color versions of one or more figures in this article are available at https://doi.org/10.1109/TMTT.2021.3129520.

Digital Object Identifier 10.1109/TMTT.2021.3129520

I. Introduction

MICROWAVE detectors are very well-known components used in wireless communications. They rely essentially on a diode or a transistor that can sense the presence of the incoming microwave radiation, the level of sensitivity (i.e., minimum power detected) depending on the device itself. The literature published in this domain is so vast that it is practically impossible to give a comprehensive list of references. However, in the last years, the attention has been moving toward geometrical diodes [1], that is, diodes which are created by etching channels in a planar semiconductor/semimetal. These devices are called "self-switching diodes" (SSDs), which have been demonstrated to detect both microwaves [2]–[4] and terahertz signals [5]–[7]. An SSD is different from classical diodes, in the sense that no junctions are necessary (hence, no doping), and its physics relies upon a nonlinear current, which flows through nanometer-sized parallel channels and is controlled by field-effect phenomena. In principle, an SSD could be modeled as a 2-D field-effect transistor (FET) [8], [9] with short-circuited gate and drain. This type of devices has been fabricated using various semiconductor and 2-D electron gas (2DEG)-like materials, like AlGaN/GaN [6], GaN [7], InAs [5], graphene [2], [10], [11], and molybdenum disulfide (MoS_2) [12], [13]. Nevertheless, to the authors' knowledge, no attempt has been made so far to fabricate an SSD based on a monolayer MoS_2/monolayer graphene heterojunction, mostly due to: 1) the difficulties in the growth of MoS_2 at the wafer scale and 2) its low mobility [14]. In this respect, this article aims at overcoming this technological gap by presenting a MoS_2/graphene SSD on high-resistivity silicon (HRSi)/silicon dioxide substrate. We go beyond the actual state-of-the-art in the domain of 2-D material-based SSDs, by validating a proof-of-concept MoS_2/graphene heterojunction for microwave detection up to 10 GHz, with the best performance around the ISM 2.45-GHz band. The 2-D heterojunction-based SSDs were designed and simulated using a theoretical model and quantum atomistic/multiphysics tools, respectively; then, the devices were fabricated in coplanar waveguide (CPW) technology for straightforward on-wafer characterization without any matching network (to be implemented in the future for optimized power transfer to

the diode); finally, a complete set of dc and high-frequency measurements were carried out to extract the fundamental parameters and key performance indicators of the devices. The problem in nowadays telecommunications systems is how to include a nanoelectronic quantum physics-based device into numerical tools for the design of complex microwave front ends. The solution that this work offers relies on the need for an advanced but rigorous lumped element equivalent circuit generated by simulated or, even better, measured scattering parameters. This novel circuit approach is substantially different from the one presented in [15], where a procedure based on Foster's method for partial fraction expansion of the admittance matrix was deployed. In this case, we obtained an equivalent circuit that included negative resistances as well, the resulting fitting to the experimental data being excellent. Even if it is known that diodes with variable capacitor and tunnel diodes (as in the present work) have led to include also negative resistors (besides lumped passive elements) as circuit components in the analysis and synthesis of linear networks [16], the presence of these negative values is not desirable. For this reason, in this article, we considered an alternative approach that overcomes the latter limitations, as it will be further demonstrated.

This article is organized as follows. Section II-A presents the motivation of this work, whereas Sections II-B and II-C are dedicated to the rigorous theoretical model and to the quantum atomistic/multiphysics simulations of the 2-D heterojunction-based SSDs, respectively. Then, in Section III, the fabrication of the SSDs is summarized. Section IV provides the detail of the dc and microwave characterization of the SSDs and, finally, Section V describes a rigorous circuit model for the proposed SSDs, which uses the measured scattering parameters to create a high-frequency equivalent circuit, suitable for its exploitation in numerical tools for the design of complex front ends. Conclusions and future perspectives are given at the end.

II. Motivation, Theoretical Model, and Quantum Atomistic/Multiphysics Simulations of the 2-D Heterojunction-Based Self-Switching Diode

A. Motivation

The advent of nanoelectronics has brought with itself the need for devices with smaller size and more extended functionalities with respect to silicon-based technologies. Nanotechnology-based products are expected to be smaller, cheaper, and lighter yet more performing, and environmentally friendly, with increased energy efficiency and high-tech capabilities. That is the motivation behind the ever-increasing success of carbon-based and, in general, 2-D nanoelectronics. The so-called phase transition materials have already found applications in microwaves (e.g., antennas and switches), the metal-insulator-transition (MIT) phenomenon being described by Mott [17]. Atomically thin transition metal dichalcogenides (TMDs) are the latest MIT materials under scrutiny, and the MoS_2 monolayer (a TMD) is the most studied 2-D material after graphene. The crystal structure of MoS_2 is made of layers of molybdenum atoms sandwiched between two layers of sulfur atoms. However, MoS_2 is harsh to be grown at the wafer scale and possesses a low mobility with respect to other semiconductors (but now comparable with that of silicon, thanks to a substantially improvement in the quality of the deposition process). Despite these limitations, MoS_2 has interesting properties, namely, MoS_2 monolayer is a direct bandgap n-type semiconductor, with a bandgap of about 1.9 eV, which decreases as the number of monolayers increases (its bulk counterpart being an indirect semiconductor with a bandgap of about 1.2 eV). On the other side, graphene ("the silicon of the 21st century") is a zero-gap semimetal (which can be grown with a high quality at the wafer scale) with high room-temperature mobility (in the order of 1000 $cm^2/V \cdot s$ [14]), hence suitable for detection/rectification of microwaves up to terahertz if properly patterned at the nanoscale. Hence, the combination of these two 2-D materials in their monolayer form could benefit from their individual advantages, creating a new type of device with unprecedented properties. Furthermore, graphene is more stable in air than MoS_2 (which is subject to oxidation with the subsequent creation of MO_x compounds). By carefully selecting the vertical stack of the heterojunction and by adopting specific fabrication techniques, it is possible to mitigate the above-mentioned limitations, thus increasing the endurance, stability, and reliability of the devices.

B. Theoretical Model of the I–V Characteristic of a 2-D Heterojunction-Based Self-Switching Diode

An SSD is a two-terminal nano-diode that rectifies voltage purely based on a self-induced field-effect mechanism that does not require a third gate terminal, junction formation, or even doping. Hence, it requires a minimal-step and low-cost (i.e., minimum number of masks) fabrication process. Its functioning is based on a nonlinear current flowing through nanometer-sized channels (in parallel) regulated by lateral field-effect phenomena. The design considered here for the SSD is, as said before, a 2-D FET with short-circuited gate and drain (or as a double side-gated FET). In Fig. 1(a), a 3-D representation of the heterojunction structure can be seen, together with the HRSi/silicon dioxide (SiO_2) substrate and the gold (Au) contacts. In Fig. 1(b), the single channel (width W_{ch} and length L_{ch}) is shown, obtained by etching two isolating trenches (width W_0) in the heterojunction.

The geometrical nature of an SSD allows optimizing separately W_{ch}, L_{ch}, and W_0, as well as the number of channels in parallel. However, for ease of fabrication and due to the small dimensions of the heterojunction sample (which forced us to select few configurations of diodes integrated with CPW lines), we will consider herein only four different channel widths, that is, $W_{ch} = 30$, 50, 75, and 100 nm, whereas $W_0 \equiv W_{ch}$ and $L_{ch} \approx 1$ μm. In Fig. 1(b), we indicated with "Gate," "Drain," and "Source" the three terminals of the FET-like SSD.

The current intensity of an SSD can be modulated by proper engineering the geometry of the single channel (i.e., W_{ch}, L_{ch}, and W_0) and the number of channels in parallel. Nonetheless, an SSD requires a bandgap for voltage rectification. The key to understand the proposed 2-D heterojunction is that

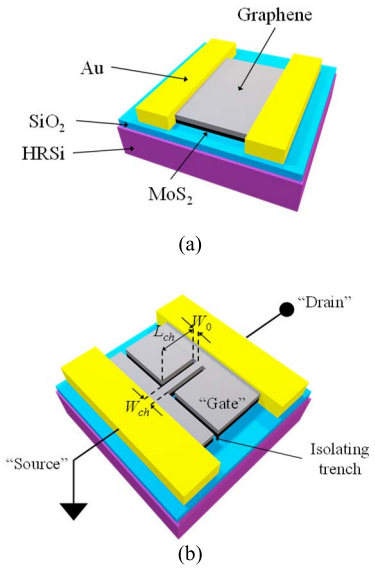

Fig. 1. (a) 3-D schematic of the MoS_2/graphene heterojunction. (b) 3-D schematic representation of a single-channel SSD based on a MoS_2/graphene heterojunction with the main dimensions.

stacked 2-D materials allow confining the charge carriers in the low bandgap material. Patterning graphene opens a small bandgap [18], [19] (between 0.05 and 0.2 eV, i.e., much smaller than MoS_2) in its Dirac dispersion with decreasing channel width and, since the channel in a MoS_2/graphene heterojunction is a narrow nanoribbon, its bandgap is expected to further increase, thanks to quantum confinement and edge effects [20]. This entails that a MoS_2/graphene heterojunction is likely to enhance the charge carrier transportation in graphene. This represents the greatest advantage of an SSD, in the sense that (as stated before) no external doping is required to achieve a diode-like behavior, and the fabrication can be performed in a few steps on any substrate that is CMOS-compatible.

An SSD can be modeled as a capacitive divider formed by a quantum capacitance C_q and a substrate capacitance C_s, connected in series (C_s is defined per each unit length). Each channel is capacitively coupled to the drain voltage through C_q and C_s. We can write the two capacitances and the total capacitance C_{tot} as follows [10]:

$$C_s = \frac{\varepsilon_0 \varepsilon_{r,\text{static}}}{W_0} \tag{1}$$

$$\varepsilon_{r,\text{static}} = \frac{\varepsilon_{r,\text{sub}} + 1}{2} \tag{2}$$

$$C_q = e^2 \rho(\mu_c) \tag{3}$$

$$C_s \ll C_q \rightarrow \frac{1}{C_{\text{tot}}} = \frac{1}{C_s} + \frac{1}{C_q} \approx \frac{1}{C_s} \tag{4}$$

where ε_0 is the vacuum's permittivity, $\varepsilon_{r,\text{static}}$ is the relative static permittivity, $\varepsilon_{r,\text{sub}}$ is the substrate's relative permittivity, e is the electron's charge, ρ is the density of states in the 2-D heterojunction, and μ_c is the chemical potential of the 2-D heterojunction. We stress here that the chemical potential of a system is the energy required to add or remove an electron from it. Together with the electron density, μ_c (which depends on an externally applied dc bias voltage) dictates how the electrons in the system are arranged. In the case of a pure graphene SSD, the drain current I_d can be expressed as follows [11]:

$$I_d \approx N \mu_{\text{eff}} C_{\text{tot}} \frac{W_{\text{ch}}}{L_{\text{ch}}} |V_d - V_D| V_d \tag{5}$$

where N is the number of channels (in the present work, $N = 12$ or, in other words, the diode can be modeled as 12 voltage-controlled current generators in parallel), μ_{eff} is the effective channel (graphene) mobility, V_d is the drain voltage, and V_D is the Dirac voltage. When $V_d > V_D$, the SSD is in forward bias (electron) condition, whereas when $V_d < V_D$ the SSD is in reverse bias (hole) condition. Equation (5) is a modified version of the well-known Shichman–Hodges model [21], which uses a controlled current source to describe I_d. However, in the proposed SSD, we must take two other issues into account, namely, 1) lattice mismatch-induced defects and 2) trapped charges at the interface between MoS_2 and graphene. For these reasons, (5) can also be used in the case of the MoS_2/graphene heterojunction in the following form:

$$I_d \approx N \mu_{2-\text{D}-\text{HJ}} C_{\text{tot}} \frac{W_{\text{ch}}}{L_{\text{ch}}} V_d^2 \tag{6}$$

where $\mu_{2-\text{D}-\text{HJ}}$ is the mobility of the 2-D heterojunction and includes all the above-mentioned phenomena linked to the superposition of two 2-D materials, and we have set (in a good approximation) $V_D = 0$ V. The crucial issue here is that stacked MoS_2 and graphene form a so-called Van der Waals (VdW) heterostructure [22], [23], in which the atoms of each layer are bound together by strong covalent bonds, whereas the planes are held together by weak VdW forces. Therefore, these materials exhibit strongly anisotropic elastic properties and the interface between two VdW layers (or between a VdW layer and the substrate underneath, i.e., MoS_2 and HRSi, respectively) is likely to be not elastically perfect. This aspect has a direct effect upon thermal and charge transport, in the sense that controlling phonon transport allows tuning the thermal conductivity [24] and the interaction of coherent phonons with charge carriers (electron and holes) has the potential to offer new perspectives in the domain of nanotechnology-based devices for the generation of microwave signals [25]. This is to say that graphene-based heterostructures need a special treatment with regard to the potential modifications in their phonon band structure, as this could lead to room-temperature values of $\mu_{2-\text{D}-\text{HJ}}$ different from the theoretically predicted upper limit for pristine graphene [26]. Finally, in Fig. 2(a), we show the equivalent circuit of the single-channel SSD and, in Fig. 2(b), the generic 3-D structure of an N-channel SSD, which can be modeled as N voltage-controlled current generators in parallel, thus increasing the total I_d.

Thanks to the semiconducting nature of MoS_2 (electron affinity $X_1 = 4$ eV and bandgap $E_g = 1.9$ eV) and to the semimetal characteristics of graphene (work function $\Phi_2 = 4.56$ eV), the MoS_2/graphene contact is of the Schottky type, with a potential barrier $\phi_B = 0.56$ eV, whereas the

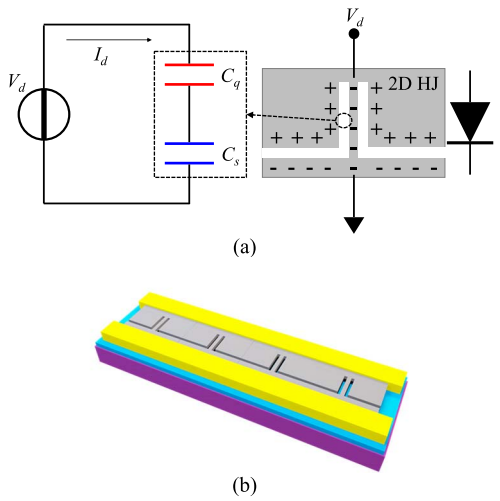

Fig. 2. (a) Circuit schematic of the capacitive divider modeling the single-channel SSD. (b) 3-D schematic of the generic multichannel SSD.

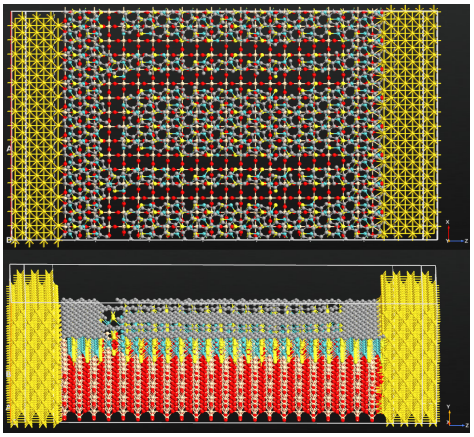

Fig. 3. Top view and lateral view of the atomistic model of a MoS_2/graphene heterojunction. Au atoms are reported in golden, while C atoms of graphene are highlighted in gray. Mo and S atoms of MoS_2 are reported in cyan and yellow, respectively; finally, the Si and O atoms are shown in light brown and red, respectively.

graphene/gold contact is characterized by a potential barrier $\phi_F = 0.54$ eV. The choice of having the MoS_2 monolayer beneath the graphene comes from the necessity of providing a rectifying behavior (Schottky contact), with charge carrier confinement into the graphene monolayer (as said before), and low contact resistance with the external metal electrodes. At the same time, the top graphene prevents the MoS_2 from oxidation, hence ensuring endurance. Moreover, since graphene monolayer exhibits ambipolar transport, we can foresee that the I–V characteristics will show a conduction mechanism for both positive and negative values of the applied dc bias. This was reported in [6] and can be interpreted by considering two main interrelating phenomena, that is, the charge neutrality near zero bias and the current saturation at high bias values. However, due to the intrinsic complexity and quantum nature of the structure under study, it is difficult to predict analytically the values of $\mu_{2-\mathrm{D}-\mathrm{HJ}}$ and C_{tot} in (6). Therefore, a much more reliable method to calculate the current-voltage dependence is using quantum atomistic/multiphysics models and simulations, as explained in detail in the following section.

C. Quantum Atomistic Simulations of a Two-Atom-Thick MoS_2/Graphene Heterojunction

Atomistic modeling and simulations have been carried out using the Quantum Atomistic Toolkit (Q-ATK) software package [27], focusing on the appropriate SSD geometry to be considered. Drain and source have been defined with two Au atomistic blocks using 110 metal layers. A middle region of 6.5 nm thickness has been optimized (Fig. 3), made of one layer of hexagonal graphene (space group 187), one layer of MoS_2 in trigonal prismatic (1H) phase (space group 194), and a 4-nm-thick layer of SiO_2 in tetragonal form (space group 136).

Two explicit channels have been modeled, with $L_{ch} = 4.6$ nm, $W_0 = 0.5$ nm, and $W_{\mathrm{ch}} = 1.2$ nm. Since it is not possible to operate a quantum atomistic model of the channels with the same dimensions of the experimental approach, the reported values have been chosen to better reproduce the experimental conditions by keeping the same order of magnitude for the geometry-dependent term $C_{\mathrm{tot}} W_{\mathrm{ch}}/L_{\mathrm{ch}}$ in (6) and, at the same time, to describe the chemical and physical properties of the heterojunction under test. A final 3-D device ($x = 5$ nm, $y = 6.5$ nm, and $z = 9$ nm) has been generated, and periodic boundary conditions (PBCs) along the x- and z-axes have been used for two purposes: 1) avoiding problems with boundary effects caused by finite size and 2) emulating the 12-channel geometry. Density functional theory (DFT) approach based on Perdew–Burke–Ernzerhof (PBE) exchange-correlation functional has been used to optimize the 3-D structure and to extrapolate the I–V characteristics of the heterojunction. To treat VdW dispersion forces between graphene and MoS_2, and between MoS_2 and SiO_2, Grimme corrective terms [28] have been included to better optimize the channel configuration. This approach is called DFT-D2 and it is characterized by higher accuracy, broader range of applicability, and lesser empiric contribution to the wave function. The long-range interlayer interactions of carbon, Mo, and S atoms have been defined, as well as interaction distances between the atoms and the interfaces. The electron basis has been expanded in a set of finite-range atomic-like basis functions following the linear combination of atomic orbital (LCAO) representation. Since the modeled channels could generate an overestimation in the energy formation, leading to artifacts, the augmented plane-wave (PAW) method combined with pair wise S–S potential has been used to extend the cut-off radius of the core-electron density for C, S, and Mo atoms, while norm-conserving pseudopotentials have been maintained for the other atom types in the model. This combined approach allowed us to obtain an optimal description of SSD geometry, avoiding the overlap between the wave function of the core electrons with the exchange correlation description, which is directly related to the valence electrons. Strong covalent bonds are formed between S and C atoms at MoS_2-graphene interfaces. The VdW interaction

TABLE I
DISTANCES BETWEEN THE ATOMS IN THE SSD ATOMISTIC MODELING

Atom types	Interatomic distances (in Å)
C-S	1.79
Mo-S	2.47
S-S	3.35
S-Si	2.31
S-O	1.91
Si-O	1.82
Si-Si	2.84
Au-Au	2.88
Au-C	1.97
Au-S	2.07
Au-Mo	1.72
Au-O	1.96
Au-Si	2.65

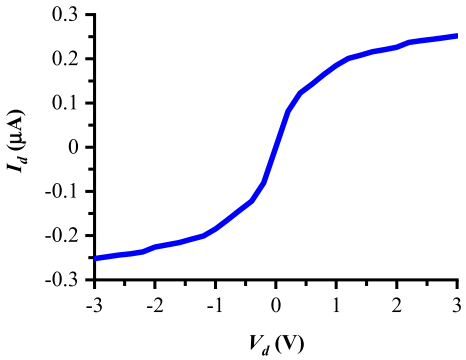

Fig. 4. Calculated I–V characteristics of a MoS_2/graphene heterojunction.

is found to play a dominant role for binding graphene with the MoS_2 layer. This suggests a weak electronic hybridization between the layers. The optimization of SSD geometry has been obtained from five interaction potentials (atom–atom, atom–ion, ion–ion, ion–electron, and electron–electron) considering distances, angles, and no bond interactions. A very stable and reliable model with two explicit channels has been obtained, because no forcing and constrictions in the bonds and interactions are detected at the extremes of the central zone, with an optimal building of the interfaces. The equilibrium geometry and the minimum energy distance between the systems have been obtained (Table I) through energy minimization of the modeled device.

After geometry optimization, the I–V characteristic of the modeled heterojunction has been calculated (Fig. 4). The DFT-D2 approach has been used again to correct inaccuracies associated with DFT-PBE eigenvalues for quasi-particle energy level alignment. This approach appears to be mandatory, since a physically motivated electron self-energy correction is necessary for the solid orbital energies in the junctions.

The simulated I–V dependence is referred to the specific transversal width of the device ($x = 5$ nm and $y = 6.5$ nm), which directly includes the 12-channel heterojunction-based SSD, since the PBCs allows repeating the two modeled channels for six times along the x-axis (thus obtaining 12 channels in parallel). This approach suggests that a quantitative

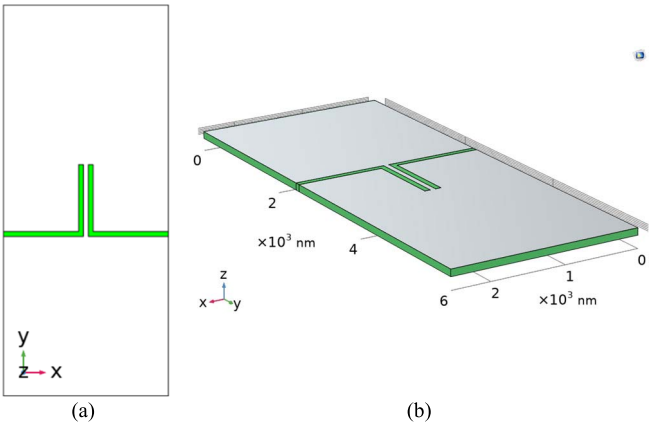

Fig. 5. Layout of the single-channel heterojunction-based SSD modeled in COMSOL Multiphysics. (a) Top view. (b) 3-D view with main dimensions.

computationally inexpensive description of coherent transport in solid junctions is readily achievable, enabling new understanding and control of charge transport properties of atomistic-scale interfaces at large bias voltages.

We stress here that the simulations with Q-ATK need a lot of time for validation, since a minimization step using different approaches should be used, as well as different algorithms for the searching of energetical local and global minima of the geometry under study. For all the previous reasons, we have resumed to COMSOL Multiphysics[1] for an easier and more comprehensive extraction of the I–V curves.

D. Multiphysics Simulations of a Two-Atom-Thick MoS_2/Graphene Self-Switching Diode

The dc modeling of the SSD has been carried out using the Semiconductor Module included in COMSOL Multiphysics, which provides a finite-element method (FEM) to solve physical problems. For simplicity, instead of simulating a complete 12-channel device, we have decided to simulate a single-channel SSD with $W_{ch} = 100$ nm (Fig. 5).

The used approach is analogous to the one showed in [29], where all the theoretical details and validation are provided. When treating the involved materials as semiconductors or dielectrics, we can apply Poisson's equation to solve charge distribution both for semiconductors and dielectric materials and drift-diffusion equations for semiconductors. An exception has been made for metal contacts, which have been handled in a particular way (illustrated later). On the other hand, graphene has been modeled as an intrinsic semimetal, with electron affinity of 4.92 eV, electron/hole mobility of 500 $cm^2/V \cdot s$, relative permittivity of 4, thickness $t_G = 0.33$ nm, and doping concentration $N_G = \alpha_n\ (2 \times 10^{11}[1/cm^2]/t_G)$ (where $0 < \alpha_n \leq 1$ is a scale factor for the effective carrier concentration that is not known *a priori*). Regarding metal contacts, we have modeled only the interface between the metal and semiconductor by means of a Schottky barrier, thus ignoring the ohmic losses that, although being present, are negligible in the dc regime. The material properties considered for MoS_2 are reported in Table II.

[1]Registered trademark.

TABLE II
MATERIAL PROPERTIES USED IN COMSOL MULTIPHYSICS FOR MoS_2

Property	MoS_2
Bandgap	1.9 eV
Electron affinity	4.3 eV
Electron mobility	200 $cm^2/V{\cdot}s$
Hole mobility	200 $cm^2/V{\cdot}s$
Relative permittivity	4.2
Monolayer thickness	0.7 nm
Electron concentration	$N_{MoS2} = \alpha_n(2{\times}10^{12}[1/cm^2]/t_{MoS2})$
Richardson's constant	$4\pi e k_B^2 m_{MoS2}{}^*/h^3$

In Table II, N_{MoS2} is the doping concentration for MoS_2, t_{MoS2} is the thickness of MoS_2, k_B is Boltzmann's constant, m^*_{MoS2} is the effective mass for electrons/holes of MoS_2, and h is Planck's constant. As mentioned before, the electrical quantities inside semiconductor materials are computed using the drift-diffusion model in combination with Poisson's equation, the latter being used also to apply charge conservation in dielectric materials (i.e., HRSi, SiO_2, and hydrogen silsesquioxane or HSQ, whose role is to protect the heterojunction), by providing a given value of the relative permittivity. To introduce a free carrier concentration in the semiconductors/semimetals, we have used an n-type analytic doping model assuming complete ionization and the doping concentrations N_G and N_{MoS2}. As stated above, the metal contacts have been modeled with Schottky barriers to simulate the typical saturation behavior visible in the I–V characteristics for this kind of devices. In this respect, the interface requires two inputs: the metal work function and Richardson's coefficient of the semiconductor (which depends on its effective mass).

Finally, Fig. 6(a) shows the simulated current-voltage dependence for $W_{\mathrm{ch}} = 100$ nm and $\alpha_n = 1$. It is worth pointing out that the following results refer to a 12-channel heterojunction-based SSD, since the current output of the single-channel diode has been multiplied by 12 in postprocessing (remember that the 12 channels are voltage-controlled current generators in parallel). As expected, one can see immediately from Fig. 6(a) that the I–V characteristic: 1) saturates due to the presence of the Schottky barriers in the contact regions and 2) exhibits a slight asymmetry, since the simulated structure is asymmetric. On the other hand, Fig. 6(b) displays a parametric sweep on the free carrier concentrations (N_G and N_{MoS2}) performed by varying α_n. The simulated results show how this property can considerably change the rectifying characteristics of a geometrical diode. In detail, it is apparent that the asymmetry increases by decreasing the electron concentration.

III. FABRICATION OF THE 2-D HETEROJUNCTION-BASED SELF-SWITCHING DIODES

In Fig. 7(a) and (b), two optical photographs of the fabricated heterojunction-based SSDs are shown, whereas Fig. 7(c) is a scanning electron microscope (SEM) picture offering a magnified view of the diode.

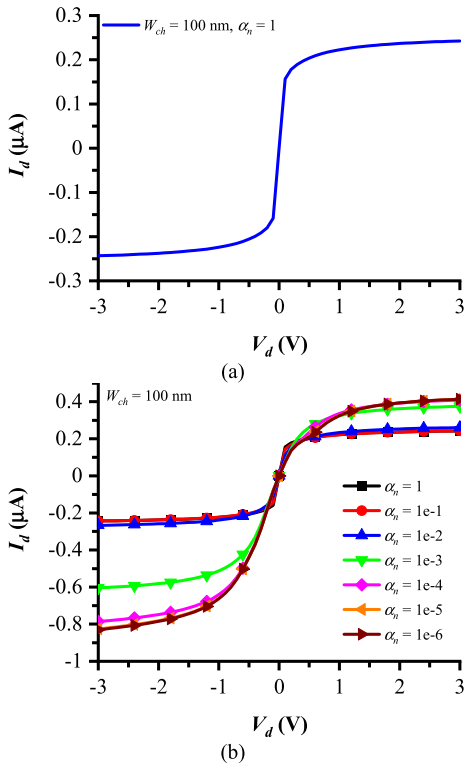

Fig. 6. Simulated I–V characteristics of a heterojunction-based SSD ($W_{\mathrm{ch}} = 100$ nm) in the $[-3, +3]$ V voltage range for (a) $\alpha_n = 1$ and (b) $\alpha_n = 1\mathrm{e} - 6, \ldots, 1\mathrm{e} - 1$.

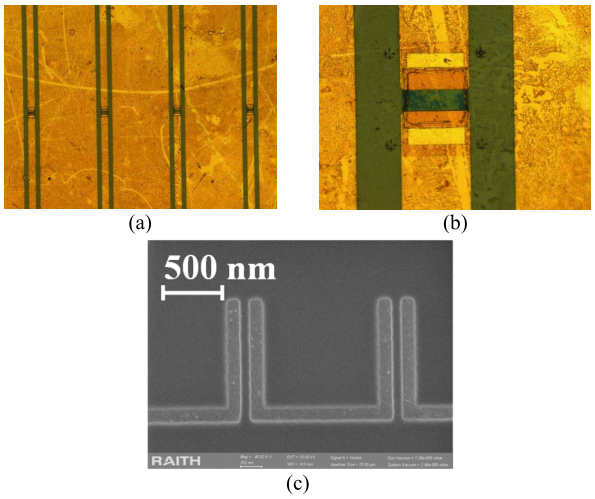

Fig. 7. (a) and (b) Optical pictures of the SSDs in CPW technology. (c) SEM photograph showing the etched channels in the MoS_2/graphene heterojunction.

For the fabrication of the 2-D heterojunction-based SSDs, some customized samples were purchased from 2-D Semiconductors (Scottsdale, AZ, USA), namely 1×1 cm^2 2-D heterojunctions made of SiO_2/HRSi (SiO_2 thickness of 90 nm, and HRSi wafer with thickness of $\sim$500 μm, and resistivity $\rho \sim 10\,000\ \Omega \cdot$ cm), monolayer MoS_2 (on SiO_2/HRSi), and monolayer graphene (on MoS_2). As in the case of plasma-enhanced chemical vapor deposition (PECVD), atmospheric pressure CVD techniques (APCVD, used for the 2-D

heterojunctions under study) can be used at different temperatures, depending on the substrate and the type of material deposited on it. In this respect, an APCVD process can cover temperatures between 100 °C and 1000 °C, meaning that it can be suitable for CMOS-compatible devices. The fabrication involved four steps: 1) deposition of metal pads by a lift-off process, in order to define diodes' areas and to improve the layers' adhesion to the SiO_2/HRSi substrate; 2) diodes' patterning using an electron-beam lithography (EBL) process and manufacturing by dry etching; 3) to avoid any damage to the heterojunctions, the diodes were covered by a negative electronresist (HSQ); and 4) manufacturing of the CPW lines (Ti/Au with total thickness of 250 nm) by a lift-off process. As stated before, the choice of using SSDs embedded into CPW lines was taken to easily perform on-wafer both dc measurements and high-frequency characterization. We fabricated four types of diodes with four different values of the channel width (i.e., $W_{\text{ch}} = 30$, 50, 75, and 100 nm), but with the same channel length $L_{\text{ch}} \approx 1\ \mu$m and the same number of channels in parallel $N = 12$.

IV. DC and Microwave Characterization of the 2-D Heterojunction-Based Self-Switching Diodes

A. DC Measurements

The dc measurements (Fig. 8) have been performed using a Keithley SCS 4200 characterization system, connected to a SÜSS MicroTec measuring platform. Of the 16 fabricated structures, 13 (81%) presented no exfoliation issues of the Au layer (this exfoliation being due to a localized problem occurred in the lift-off process). The diodes with the highest dc current I_d in dark conditions are the ones with $W_{\text{ch}} = 100$ nm, followed by $W_{\text{ch}} = 75$, 50, and 30 nm as predicted by (6); however, when providing a white light with 100% intensity, the best performing SSDs are those with $W_{\text{ch}} = 75$ nm (in this case, the difference between 75 and 100 nm in the I_d values being of 13%).

Fig. 8 presents a comprehensive view of the simulated and measured I–V characteristics. In Fig. 8(a), one can notice that, in the range $[-3, +3]$ V of the applied dc voltage V_d, the agreement between multiphysics simulations (for $\alpha_n = 1\text{e} - 3$) and measured results is very good, with the heterojunction behaving like a slightly asymmetric "back-to-back" diode, thanks to: 1) the semiconducting nature of the MoS_2 monolayer; 2) the ambipolar conduction mechanism of graphene; and (3) the double Schottky contact between metal and heterojunction, with I_d attaining values between -500 and 400 nA. This outcome also confirms the fact that both MoS_2 and graphene have been modeled correctly inside COMSOL Multiphysics. Furthermore, since MoS_2 is a light- and infrared-sensitive semiconductor, the application of a white light source of variable intensity allows increasing I_d up to 2.6 times. This photoconductive effect can be attributed to trapping of carriers in band tail states in conduction and valence bands because of structural defects in MoS_2 itself (or induced by disorder), because these band tail states exist underneath (above) the conduction (valence) band edge, acting as electron (hole) charge traps [30]. Fig. 8(b) presents the

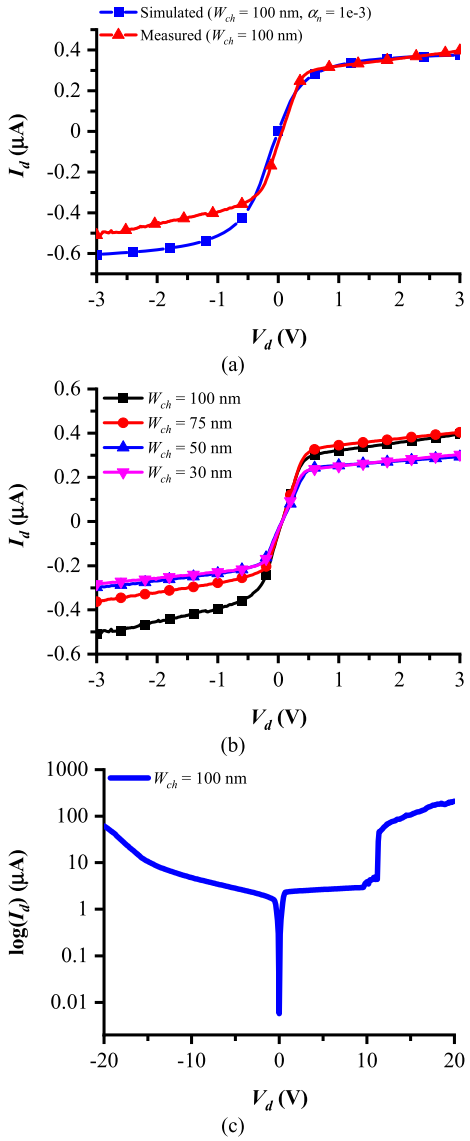

Fig. 8. (a) Simulated ($\alpha_n = 1\text{e} - 3$, solid blue curve with squares) and measured (solid red curve with triangles) I–V characteristics of the heterojunction-based SSD ($W_{\text{ch}} = 100$ nm) in the $[-3, +3]$ V voltage range. (b) Measured I–V curves as a function of channel width. (c) Measured I–V characteristic between -20 and $+20$ V (vertical axis: log-scale) of the heterojunction-based SSD with $W_{\text{ch}} = 100$ nm. All the presented curves have been obtained in dark conditions, that is, without any illumination.

measured I–V curves as a function of W_{ch}, in the range $[-3, +3]$ V. As stated before, the highest dc current (in dark conditions) is the one associated with $W_{\text{ch}} = 100$ nm (this is especially visible for negative bias voltages). Finally, from Fig. 8(c), one can observe that at $+10$ V, the SSD behaves as a tunnel diode, with an abrupt increase of the dc current up to hundreds of microamperes (hence of a factor 1000). A possible explanation of such phenomenon is the joint effect of MoS_2 bandgap, geometry-induced bandgap in graphene, and charge trapping at the MoS_2/graphene interface. Repeated measurements spanning between -20 and $+20$ V have shown a constant behavior of the diode and have not caused any performance degradation. This result is remarkable, in the sense that such a diode exhibits robust functioning conditions

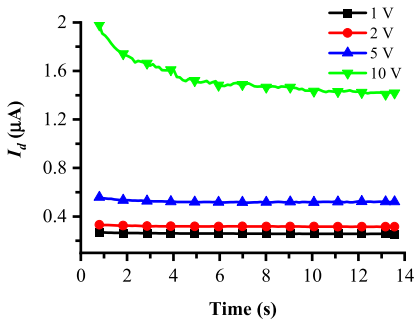

Fig. 9. Measured I_d as a function of time, for different values of the applied voltage V_d. The increase of I_d is evident, and it is a direct result of the specific conduction mechanism of the heterojunction.

in terms of insensitivity to potentially dangerous voltage outbursts. Besides this aspect, the performed measurements have confirmed that the breakdown voltage is much higher than ±6 to 7 V as in the case of pure graphene-based SSDs [2], [11] or pure multi-layer MoS_2-based SSDs [12], which already exhibited better performance than the state-of-the-art SSDs available so far. The abrupt increase of I_d when applying $V_d = 10$ V is apparent in Fig. 9, where I_d is represented as a function of time and V_d: the steady-state values of I_d for $V_d = 10$ V are 6 times bigger with respect to the case $V_d = 1$ V. It is worth noticing that the initial transient behavior is likely due to the capacitive part of the diode, whereas a possible explanation for the steady state being reached after several seconds relies in the time needed by the excess charges trapped inside the heterojunction itself to be released inside the device.

Microwave detection using SSDs is possible if the I–V characteristic is nonlinear. The most significant performance indicators of any detector are the differential resistance R_d (in Ω), the sensitivity γ (in V^{-1}), and the noise equivalent power NEP (in pW/$\sqrt{}$Hz), defined as follows:

$$R_d = 1/(\partial I_d/\partial V_d) \tag{7}$$

$$\gamma = \left(\partial^2 I_d/\partial V_d^2\right)/(\partial I_d/\partial V_d) \tag{8}$$

$$\text{NEP} = \sqrt{4k_B T R_{d0}}/\beta_{Z_{\text{RF}}} \tag{9}$$

where T is the temperature (in K), $R_{d0} = R_d(V_d = 0\ \text{V})$, and $\beta_{Z_{\text{RF}}}$ is the voltage responsivity with an RF source of impedance Z_{RF}. We stress here that (9) is valid under the assumption that the microwave detection occurs at zero bias, that is, Johnson–Nyquist noise (or thermal noise) is the dominant contribution. For the voltage responsivity $\beta_{Z_{\text{RF}}}$, we can express in a twofold manner: 1) $\beta_{Z_{\text{RF}}} \equiv \beta_{\text{low}} \approx |-2\gamma\,\text{Re}\{Z_{\text{RF}}\}|$ at low frequencies and if $R_d \gg \text{Re}\{Z_{\text{RF}}\}$ and 2) $\beta_{Z_{\text{RF}}} \equiv \beta_{\text{high}} = |-0.5 R_d \gamma\,(1-|S_{11}|^2)|$, where S_{11} is the reflection coefficient at the input port of the SSD. Assuming $T = 290$ K and $Z_{\text{RF}} = 50\ \Omega$, at zero bias the heterojunction-based SSD exhibits the following performance, summarized in Table III, where NEP_{low} is the NEP calculated with the responsivity β_{low}.

From Table III, it can be seen that the zero-bias differential resistance is quite high, as expected for such a device, but the nonzero sensitivity allows zero-bias microwave detection. Finally, Fig. 10 shows the values of R_d and γ in the voltage range [−0.2, 0.2] V (which is of interest for low-voltage detection). From Fig. 10, it is evident how R_d reaches its maximum value for $V_d \neq 0$ V, which means that the Dirac voltage $V_D \approx 50$ mV and the overall heterojunction is n-type. At the same time, in the interval [−0.2, 0.2] V, the values of NEP_{low} vary between 0.13 and 2.52 nW/$\sqrt{}$Hz, hence good values in line with the state-of-the-art SSDs available so far.

TABLE III

MAIN PERFORMANCE OF THE HETEROJUNCTION-BASED SSD AT ZERO-BIAS AND AT LOW FREQUENCIES

Parameter	Value at $V_d = 0$ V
Differential resistance R_d	2.05 MΩ
Sensitivity γ	≈ 0.5 V^{-1}
Low-frequency responsivity β_{low}	102.74 V/W
Low-frequency noise equivalent power NEP_{low}	1.77 nW/√Hz

TABLE IV

COMPARISON BETWEEN THE PROPOSED HETEROJUNCTION-BASED SSD AND THE STATE-OF-THE-ART MICROWAVE DETECTORS

Ref.	Type of diode	f_0 or B_f (GHz)	Responsivity	NEP (pW/√Hz)
[31]	SMS7630-079LF	5	5500 mV/mW	1.49
[32]	Spin-torque microwave diode	5	(V_{det} = -8 μV)	–
[33]	JFET ATF-38143-BLKG	2.45	~5 mV/mW	–
[34]	HSMS282R	1.8–2.7	1.57 mV/μW	–
[35]	Skyworks SMS7630-079LF	1–11	~1000 mV/mW at 3 GHz	–
[36]	Few-layer MoS_2 Schottky diode	0.1–2.4	7.2 A/W	–
[37]	Planar-doped potential-well barrier diode	10	10900 V/W	–
[38]	Metal-insulator-graphene (MIG) diode	2.5–70	148 mV/mW	–
This work	2-atom-thick MoS_2/graphene heterojunction	2.49	7.8×10^5 V/W	0.34

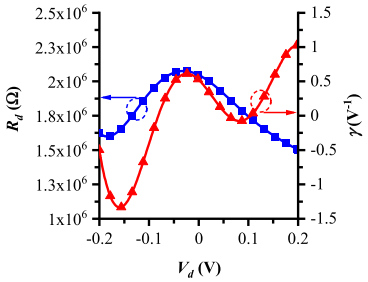

Fig. 10. Extracted differential resistance R_d (left vertical axis, blue solid line with squares) and sensitivity γ (right vertical axis, solid red line with triangles), in the voltage range [−0.2, 0.2] V, of the fabricated heterojunction-based SSD.

B. Microwave Measurements

In Fig. 11, we present the measured scattering (S) parameters [Fig. 11(a), Smith chart representation] and the calculated

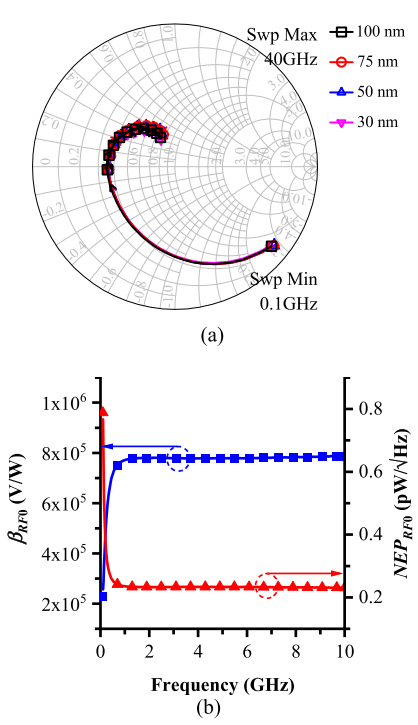

Fig. 11. (a) Measured scattering parameters in the band 0.1–40 GHz and for an input power of −23 dBm. (b) Calculated zero-bias voltage responsivity β_{RF0} (left vertical axis, blue solid line with squares) and noise equivalent power NEP_{RF0} (right vertical axis, solid red line with triangles) of the fabricated heterojunction-based SSD, in the band 0.1–10 GHz and for an input power of −23 dBm.

zero-bias frequency-dependent (up to 10 GHz) voltage responsivity β_{RF0} and noise equivalent power NEP_{RF0} [Fig. 11(b)], left and right vertical axes, respectively], using the formulas $\beta_{RF0} = |-0.5R_{d0}\gamma_0(1-|S_{11}|^2)|$ and $NEP_{RF0} = (4k_BTR_{d0})^{1/2}/\beta_{RF0}$ (where γ_0 is the zero-bias sensitivity). More in detail, the S-parameters of the two-port SSD have been measured with a vector network analyzer (VNA, Anritsu 37397D, equipped with internal bias tees), over the band 0.1–40 GHz to cover the entire microwave and part of the millimeter-wave spectrum; this choice was made to extract an ultra-wideband equivalent circuit of the SSD, as it will be explained in Section V. The S-parameter measurements have been performed using a probe station (SÜSS MicroTec) with ground–signal–ground (GSG) probe tips. Before carrying out any microwave measurements, we have also performed a standard SOLT (=short-open-load-thru) calibration for proper de-embedding of the reflection (S_{11}) and transmission (S_{21}) coefficients. The input power P_{in} was just −23 dBm (i.e., to operate in small-signal regime), meaning that the delivered power $P_{del} = P_{in}(1-|S_{11}|^2)$ was between −29.4 dBm (at 0.1 GHz) and −23.24 dBm (at 40 GHz). The Smith chart shows that the SSD has a capacitive-type input reactance X_{11} in the band 0.1–4.75 GHz, whereas X_{11} becomes the inductive type from 4.75 to 40 GHz. The input resistance R_{11} is between 17 and 40 Ω, whereas X_{11} falls within the range [−139, 33] Ω, with the input impedance $Z_{11} = R_{11} + jZ_{11}$ becoming purely resistive at 4.75 GHz with $R_{11} \approx 18$ Ω. From Fig. 11(b), one can see that β_{RF0} is almost constant between

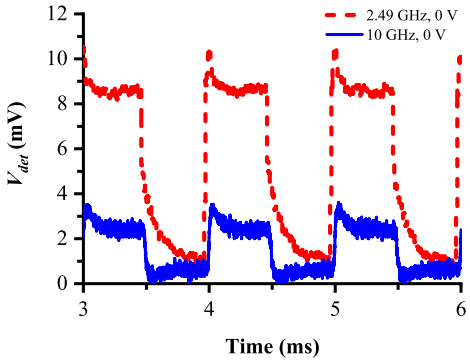

Fig. 12. Voltage V_{det} detected by the fabricated heterojunction-based SSD, as a function of time, when using a 1-kHz AM 2.49-GHz carrier (red dashed line) and a 10-GHz carrier (blue solid line) with an input power of +10 dBm and with a dc bias of 0 V.

1 and 10 GHz, whereas NEP_{RF0} decreases with frequency and exhibits excellent values between 0.2 and 0.8 pW/√Hz.

The detection capabilities of the heterojunction-based SSDs have been measured by using a microwave generator (Agilent E8257D) to transmit an AM carrier frequency between 900 MHz and 10 GHz. The input power P_{in} has been varied between −1 and +10 dBm. The frequency of the rectangular shape modulating signal has been set to 1 kHz. The output of the diode has been registered by a digital oscilloscope (Tektronix DPO 2024 with noise reject) connected to a load resistance of 1 MΩ. A dc external source (Agilent E3631A) has been deployed to bias the diode (in the range [0, +1] V) through a bias tee (Marki BT0040). In Fig. 12, it is shown the detected dc voltage V_{det} at 2.49 GHz (best case) and at 10 GHz, for $P_{in} = +10$ dBm (large-signal regime) and a bias of 0 V. Since the attenuation of the coaxial cable connecting the microwave generator to the CPW probe tips at diode's input port is between 0.38 and 0.76 dB in the band 2.49–10 GHz, it means that the real input power $P_{in,real}$ is equal to 9.62 dBm at 2.49 GHz and to 9.22 dBm at 10 GHz, and the delivered power is $P_{del} \approx P_{in,real}(1-|S_{11}|^2)$ (hence, spanning between 8.17 and 8.51 dBm). The maximum V_{det} is about 10 mV at 2.49 GHz (and it increases up to about 65 mV with a dc bias of +1 V), whereas at 10 GHz the maximum V_{det} is about 4 mV. These are the best results obtained so far, since at higher frequencies and power values V_{det} undergoes distortion phenomena, likely due to intermodulation products and supplementary thermal and/or $1/f$ noise. The input power of +10 dBm allows maximizing the microwave detection of the diode and gives a proof of the maximum power level sustained by the SSD without distorting V_{det}. Moreover, the proposed 2-D heterojunction does not exhibit any deterioration of its performance during repeated measurements, likely because (as shown previously) the diode is able to sustain high dc bias voltage values (i.e., at least ±20 V and maybe more). We also stress here that we have repeated the microwave characterization of the diodes more than one year after their fabrication and the performance is practically the same: this is an evident proof of the importance of capping the monolayer MoS_2 with monolayer graphene, as the strong covalent bonds of graphene and its stability in air at room temperature prevent potential oxidation issues of the underneath MoS_2.

Finally, Table IV presents a comparison between the proposed heterojunction-based SSDs and some of the latest works in the literature regarding microwave detectors. In Table IV, f_0 (B_f) is the reference frequency (frequency band). One can see how the MoS_2/graphene diode exhibits excellent performance with respect to the available state-of-the-art, in terms of both responsivity and NEP (for the latter, many articles do not even report its value, which is an important indicator of the noise introduced by the device). Hence, we can state that this is a further proof of the potential offered by atomic-scale materials for microwave applications.

From the measured scattering parameters, one can extract a rough frequency-dependent $R_{eq}C_{eq}$ parallel equivalent circuit in a small band, namely 0.1–4 GHz (as to cover the reference 2.45 ISM band). In this case, R_{eq} attains the values 680 Ω (at 0.1 GHz)–18 Ω (at 4 GHz), whereas C_{eq} spans the range 11 pF (at 0.1 GHz)–0.14 pF (at 4 GHz). Hence, a matching circuit will be envisaged in the future for optimal power transfer to the SSD. Beside this, to model in a very rigorous way the heterojunction-based SSD, it is necessary to resume to a more sophisticated equivalent circuit: this will be explained in detail in the following section.

V. Equivalent Circuit of the 2-D Heterojunction-Based Self-Switching Diode

The identification of an equivalent network for lossless two-port device is quite simple, as discussed and analyzed in Marcuvitz and Montgomery handbooks [39], [40]. In fact, if we embed a diode (or another microwave discontinuity) into a CPW line, we can represent the global device as the "series" of: 1) the input transmission line with proper electrical length (i.e., the CPW section from the input port to the diode); 2) an equivalent circuit representing the diode (just like, e.g., two transmission lines embedding a shunt load); and 3) the output transmission line with proper electrical length (i.e., the CPW section from the diode to the output port).

The presence of losses in the device makes the identification process quite complex. Carlin and Youla [16], [41] showed that a lossy two-port device can be identified with a circuit containing lumped capacitances, inductances, transformers, and resistances, that can be positive or negative. On the other hand, those circuits do not consider the effect of wave propagation in microwave devices that are usually represented by transmission lines. Recently [42], a new identification process has been applied to lossy devices that combines the presence of transmission lines, two positive resistances (representing the losses), and a shunt load, as shown in Fig. 13 for symmetric devices. The number of parameters is exactly the minimum number that can be used to represent a lossy symmetric device. In fact, for such device, the scattering matrix has four independent parameters: amplitude and phase of S_{11} and S_{21}, with $S_{22} = S_{11}$ by symmetry. In this sense, apart from the representation of the shunt load with one or more shunt branches, we recognize exactly four independent parameters (the external θ^c and internal θ^x electrical lengths, the resistance R, and the susceptance B) that correspond just to four independent parameters. In this sense, the proposed circuit representation is minimal because it contains the minimum number of independent parameters.

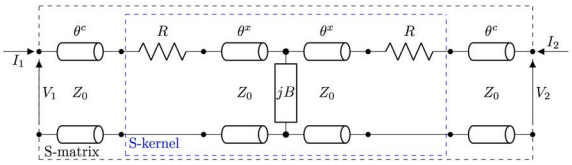

Fig. 13. Equivalent network for two-port lossy devices.

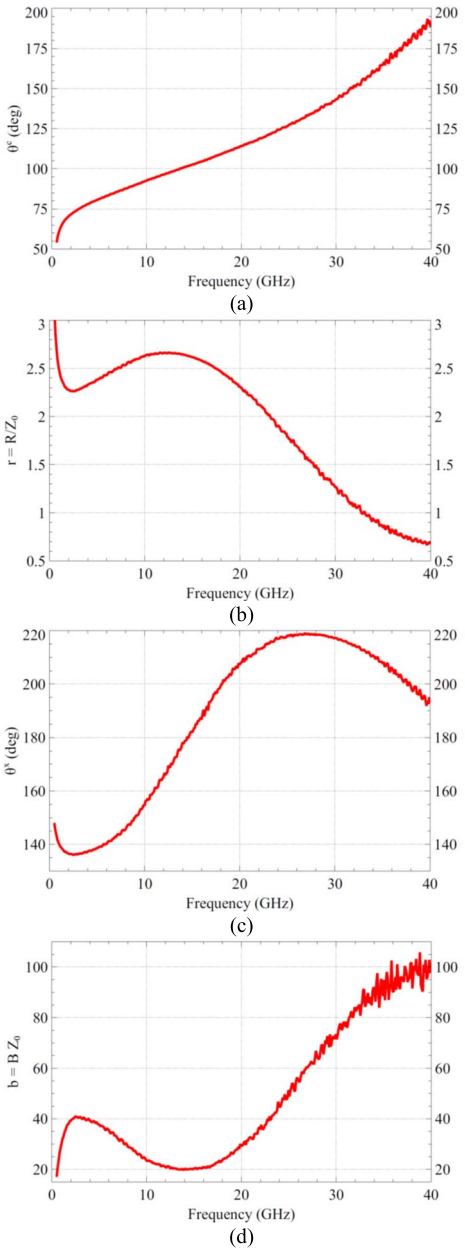

Fig. 14. Electrical parameters of the equivalent network of the SSD measured S-matrix. (a) External electrical length θ^c. (b) Normalized resistance r. (c) Internal electrical length θ^x. (d) Normalized susceptance b.

The proposed equivalent network is based on the transformation of the measured/simulated scattering matrix ("S-matrix" in Fig. 13) in a new scattering matrix of the

TABLE V

VALUES OF THE INDUCTANCES AND CAPACITANCES FOR THE MODELED SUSCEPTANCE b SHOWN IN THE LAST COLUMN

Band	L_1 (pH)	C_1 (pF)	L_2 (pH)	C_2 (pF)	Circuit schematic
UHF	–	102.51	–	–	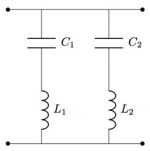
L	-45.85	112.81	–	–	
S	-34.54	92.71	–	–	
C	-27.66	69.25	–	–	
X	-30.83	116.94	–	–	
K_u	–	3.66	-336.36	-0.69	
$K+K_a$	–	9.92	12.09	–	

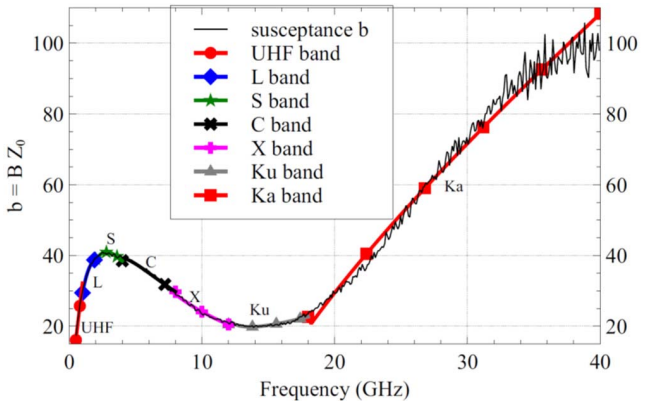

Fig. 15. Comparison between the identified (black line, for the component that can be seen from Fig. 13) and modeled (various colors and styles, solid thick lines, for the network that can be seen in the last column of Table V) normalized susceptance b.

kernel ("S-kernel") that can be separated in lossy and lossless parts, by means of external transmission lines with a proper electrical length θ^c. The lossy part is represented by resistances which are both positive, being relative to a positive definite Hermitian matrix, while the lossless part is represented by the classical network of [39], [40], and [42], constituted by a shunt load and two transmission lines with electrical length θ^x. The identification process has been applied to the measured scattering parameters and the obtained electrical lengths, the normalized resistance r and the normalized susceptance b are shown in Fig. 14. This approach is correct even in the presence of a nonlinear device (i.e., the heterojunction-based SSD), since the latter was measured in terms of a 2-port S-matrix in small-signal regime, at a power level of −23 dBm.

The normalized shunt susceptance b [Fig. 14(d)] shows a particular behavior that can be recognized not in a single component but in a combination of shunt branches. The whole band 0.1–40 GHz is divided in the IEEE standard frequency bands and the shunt load is approximated in each band by means of one or two shunt branches as reported in Table V. The corresponding behavior of the modeled shunt load is shown with different colors, each for each band, in Fig. 15.

The presence of negative inductances and/or capacitances in some bands must not surprise, because it is typical of non-Foster network, where the slope of the reactance/susceptance is negative [43].

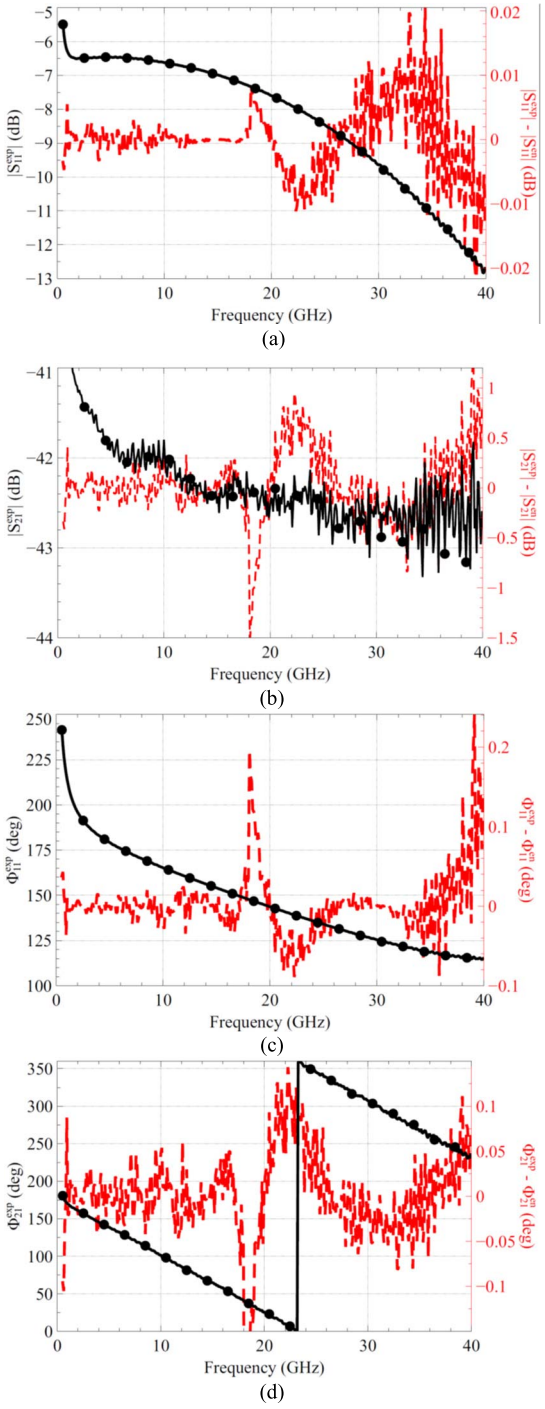

Fig. 16. (a) and (b) Amplitudes and (c) and (d) phases of the scattering parameters of the experimental results (left vertical axes, solid black lines with circles) and difference between experimental and equivalent network S-matrices (right vertical axes, dashed red lines).

It should be noted that an approximated circuit that covers the whole band 0.1–40 GHz can be obtained by adding a third branch to the modeled shunt load of Table V. The third branch is constituted by a series of an inductance and two parallel LC blocks with reactive elements that vary with frequency, as occurs in other structures analyzed in [44]. This case is not reported here because the division in the IEEE bands seems more effective.

Finally, Fig. 16 shows the comparison between the experimental S-matrix (S^{exp}) and the S-matrix reconstructed in the IEEE bands of interest by the equivalent network (S^{en}) with the modeled shunt load. The difference (red lines) between S^{exp} and S^{en}, shown in the right axis of the four plots, is extremely low, showing a particularly good agreement for the identified equivalent network with the modeled susceptance shown in Table V.

The experimental *S*-matrix shows: 1) the reflection coefficient [Fig. 16(a)] that could be improved by adding a matching network (for optimal power transfer to the diode), not yet designed at this stage because the real electrical behavior of the heterojunction-based SSD had to be accurately measured and 2) the low transmission coefficient [Fig. 16(b)], probably due to: 1) ohmic losses (related to the metal layers that are very thin with respect to skin depth of gold) and 2) the intrinsic dissipative nature of the diode embedded into the CPW signal line. Both aspects must be considered to try to improve transmission for further enhancement of the performance, together with the technological constraints of fabrication process. In this respect, the thin metal layer is a prerequisite to avoid potential exfoliation problems of the Au deposition, as this problem is likely to be encountered for thicknesses greater than 300 nm. Considering that the penetration depth in the considered band (i.e., 0.1–40 GHz) is between 0.38 and 7.53 μm, it is apparent how ohmic losses can have a significant impact on the overall transmission properties evidenced by the measured two-port S-matrix of the diode.

VI. Conclusion

In this article, we have presented the theoretical modeling, quantum atomistic/multiphysics simulations, design, fabrication, dc/high-frequency characterization, and circuit modeling of an SSD based on a MoS_2/graphene heterojunction, which can be reproduced at the wafer scale, thanks to its CMOS compatibility and ease of fabrication. This article tries to give a comprehensive solution to the problem of how to include a nanoelectronic quantum physics-based device into numerical tools for design of complex microwave front ends. For this reason, we propose a novel approach based on a rigorous lumped element equivalent circuit for lossy two-port devices in small-signal regime. In particular, the new identification process uses the measured scattering parameters and combines the presence of transmission lines, two positive resistances (representing the losses), and a shunt load. The experimental results prove that the heterojunction can be used efficiently as a microwave detector up to 10 GHz, with the best performance around the ISM 2.45-GHz band. In conclusion, this article provides the demonstration of how 2-D materials can be integrated profitably into modern and future electronics and, in this respect, the equivalent circuit is a powerful tool to model such devices in a standard circuit simulator.

References

[1] A. M. Song, M. Missous, P. Omling, A. R. Peaker, L. Samuelson, and W. Seifert, "Unidirectional electron flow in a nanometer-scale semiconductor channel: A self-switching device," *Appl. Phys. Lett.*, vol. 83, no. 9, pp. 1881–1883, Aug. 2003.

[2] A. Westlund *et al.*, "Graphene self-switching diodes as zero-bias microwave detectors," *Appl. Phys. Lett.*, vol. 106, no. 9, Mar. 2015, Art. no. 093116.

[3] C. Balocco *et al.*, "Microwave detection at 110 GHz by nanowires with broken symmetry," *Nano Lett.*, vol. 5, no. 7, pp. 1423–1427, Jun. 2005.

[4] H. Sanchez-Martin *et al.*, "Microwave detection up to 43.5 GHz by GaN nanodiodes: Experimental and analytical responsivity," in *Proc. Spanish Conf. Electron Devices (CDE)*, Feb. 2017, pp. 1–4.

[5] A. Westlund *et al.*, "Terahertz detection in zero-bias InAs self-switching diodes at room temperature," *Appl. Phys. Lett.*, vol. 103, no. 13, Sep. 2013, Art. no. 133504.

[6] P. Sangaré *et al.*, "Experimental demonstration of direct terahertz detection at room-temperature in AlGaN/GaN asymmetric nanochannels," *J. Appl. Phys.*, vol. 113, no. 3, Jan. 2013, Art. no. 034305.

[7] H. Sánchez-Martín *et al.*, "GaN nanodiode arrays with improved design for zero-bias sub-THz detection," *Semicond. Sci. Technol.*, vol. 33, no. 9, Aug. 2018, Art. no. 095016.

[8] B. Hähnlein, B. Händel, J. Pezoldt, H. Töpfer, R. Granzner, and F. Schwierz, "Side-gate graphene field-effect transistors with high transconductance," *Appl. Phys. Lett.*, vol. 101, no. 9, Aug. 2012, Art. no. 093504.

[9] M. Åberg, J. Saijets, A. Song, and M. Prunnila, "Simulation and modeling of self-switching devices," *Phys. Scripta*, vol. 2004, no. T114, pp. 123–126, 2004.

[10] M. Winters, M. Thorsell, W. Strupiński, and N. Rorsman, "High frequency electromagnetic detection by nonlinear conduction modulation in graphene nanowire diodes," *Appl. Phys. Lett.*, vol. 107, no. 14, Oct. 2015, Art. no. 143508.

[11] M. Yasir *et al.*, "Integration of antenna array and self-switching graphene diode for detection at 28 GHz," *IEEE Electron Device Lett.*, vol. 40, no. 4, pp. 628–631, Apr. 2019.

[12] M. Dragoman *et al.*, "MoS_2 radio: Detecting radio waves with a two-dimensional transition metal dichalcogenide semiconductor," *Nanotechnology*, vol. 31, no. 6, Nov. 2019, Art. no. 06LT01.

[13] M. Dragoman *et al.*, "Multifunctionalities of 2D MoS_2 self-switching diode as memristor and photodetector," *Phys. E, Low-Dimensional Syst. Nanostruct.*, vol. 126, Feb. 2021, Art. no. 114451.

[14] S. H. Mir, V. K. Yadav, and J. K. Singh, "Recent advances in the carrier mobility of two-dimensional materials: A theoretical perspective," *ACS Omega*, vol. 5, no. 24, pp. 14203–14211, Jun. 2020.

[15] M. Aldrigo *et al.*, "Microwave detection using 2-atom-thick heterojunction diodes," in *IEEE MTT-S Int. Microw. Symp. Dig.*, Atlanta, GA, USA, Jun. 2021, pp. 315–318.

[16] H. J. Carlin and D. C. Youla, "Network synthesis with negative resistors," *Proc. IRE*, vol. 49, no. 5, pp. 907–920, May 1961.

[17] N. F. Mott, "Metal-insulator transition," *Rev. Mod. Phys.*, vol. 40, no. 4, pp. 677–683, Oct. 1968.

[18] M. Dragoman, A. Dinescu, F. Nastase, and D. Dragoman, "Memtransistors based on nanopatterned graphene ferroelectric field-effect transistors," *Nanomaterials*, vol. 10, no. 7, p. 1404, Jul. 2020.

[19] M. Dragoman, A. Dinescu, F. Nastase, A. Moldovan, and D. Dragoman, "Graphene bandgap induced by ferroelectric HfO_2 doped with Zr (HfZrO)," *Nanotechnology*, vol. 31, no. 27, Apr. 2020, Art. no. 275202.

[20] S. Harrison *et al.*, "Heterodimensional charge-carrier confinement in stacked submonolayer InAs in GaAs," *Phys. Rev. B, Condens. Matter*, vol. 93, no. 8, Feb. 2016, Art. no. 085302.

[21] H. Shichman and D. A. Hodges, "Modeling and simulation of insulated-gate field-effect transistor switching circuits," *IEEE J. Solid-State Circuits*, vol. JSSC-3, no. 3, pp. 285–289, Sep. 1968.

[22] A. K. Geim and I. V. Grigorieva, "Van der Waals heterostructures," *Nature*, vol. 499, no. 7459, pp. 419–425, 2013.

[23] A. C. Ferrari *et al.*, "Science and technology roadmap for graphene, related two-dimensional crystals, and hybrid systems," *Nanoscale*, vol. 7, no. 11, pp. 4598–4810, Sep. 2015.

[24] S. Z. Butler *et al.*, "Progress, challenges, and opportunities in two-dimensional materials beyond graphene," *ACS Nano*, vol. 7, no. 4, pp. 2898–2926, 2013.

[25] S. L. Heywood *et al.*, "Heterodyne mixing of millimetre electromagnetic waves and sub-THz sound in a semiconductor device," *Sci. Rep.*, vol. 6, no. 1, Sep. 2016, Art. no. 30396.

[26] E. H. Hwang and S. D. Sarma, "Acoustic phonon scattering limited carrier mobility in two-dimensional extrinsic graphene," *Phys. Rev. B, Condens. Matter*, vol. 77, no. 11, Mar. 2008, Art. no. 115449.

[27] S. Smidstrup *et al.*, "QuantumATK: An integrated platform of electronic and atomic-scale modelling tools," *J. Phys., Condens. Matter*, vol. 32, no. 1, Jan. 2020, Art. no. 015901.

[28] S. Grimme, J. Antony, S. Ehrlich, and H. Krieg, "A consistent and accurate *ab initio* parametrization of density functional dispersion correction (DFT-D) for the 94 elements H-Pu," *J. Chem. Phys.*, vol. 132, no. 15, Apr. 2010, Art. no. 154104.
[29] N. Pelagalli, E. Laudadio, P. Stipa, D. Mencarelli, and L. Pierantoni, "Efficient and versatile modeling of mono- and multi-layer MoS_2 field effect transistor," *Electronics*, vol. 9, no. 9, p. 1385, Aug. 2020.
[30] M. M. Furchi, D. K. Polyushkin, A. Pospischil, and T. Mueller, "Mechanisms of photoconductivity in atomically thin MoS_2," *Nano Lett.*, vol. 14, no. 11, pp. 6165–6170, Oct. 2014.
[31] H. Wu, Y. Li, and L. Sun, "Design of 2–18 GHz zero-bias Schottky diode detector," in *Proc. Int. Appl. Comput. Electromagn. Soc. Symp.-China (ACES)*, Nanjing, China, Aug. 2019, pp. 1–2.
[32] P. Y. Artemchuk *et al.*, "Measurement of microwave signal frequency by a pair of spin-torque microwave diodes," *IEEE Magn. Lett.*, vol. 12, pp. 1–5, 2021.
[33] E. Shafah, A. Moulay, and T. Djerafi, "A 2.45 GHz signal detector based on zero biasing field effect transistor," in *Proc. 49th Eur. Microw. Conf. (EuMC)*, Paris, France, Oct. 2019, pp. 45–48.
[34] H. Zhang, J. Hu, L. Li, J. Xin, and D. Wang, "Design of LTE-band microwave power detection system based on Schottky diode," *IEEE Sensors J.*, vol. 19, no. 9, pp. 3425–3430, May 2019.
[35] A. Moulay and T. Djerafi, "Multi-stage Schottky diode power harvester for UWB application," in *Proc. IEEE Wireless Power Transf. Conf. (WPTC)*, Montreal, QC, Canada, Jun. 2018, pp. 115–119.
[36] X. Zhang *et al.*, "MoS_2 phase-junction-based Schottky diodes for RF electronics," in *IEEE MTT-S Int. Microw. Symp. Dig.*, Philadelphia, PA, USA, Jun. 2018, pp. 345–347.
[37] M. Akura, G. Dunn, and M. Missous, "A hybrid planar-doped potential-well barrier diode for detector applications," *IEEE Trans. Electron Devices*, vol. 64, no. 10, pp. 4031–4035, Oct. 2017.
[38] M. Saeed *et al.*, "0.15 mm^2, DC-70 GHz, graphene-based power detector with improved sensitivity and dynamic range," in *IEEE MTT-S Int. Microw. Symp. Dig.*, Philadelphia, PA, USA, Jun. 2018, pp. 1519–1522.
[39] C. G. Montgomery, R. H. Dicke, and E. M. Purcell, *Principles of Microwave Circuits*, 1st ed. London, U.K.: McGraw-Hill, 1987.
[40] N. Marcuvitz, *Waveguide Handbook*. New York, NY, USA: McGraw-Hill, 1951.
[41] H. J. Carlin, "On the physical realizability of linear non-reciprocal networks," *Proc. IRE*, vol. 43, no. 5, pp. 608–616, May 1955.
[42] L. Zappelli, "Equivalent circuits of lossy two-port waveguide devices," *IEEE Trans. Microw. Theory Techn.*, vol. 67, no. 10, pp. 4095–4106, Oct. 2019.
[43] D. Gregoire, C. White, and J. Colburn, "Wideband artificial magnetic conductors loaded with non-Foster negative inductors," *IEEE Antennas Wireless Propag. Lett.*, vol. 10, pp. 1586–1589, 2011.
[44] J. C. Rautio, "Synthesis of compact lumped models from electromagnetic analysis results," *IEEE Trans. Microw. Theory Techn.*, vol. 55, no. 12, pp. 2548–2554, Dec. 2007.

M. Aldrigo (Member, IEEE) received the Ph.D. degree in electronic engineering, telecommunications, and information technology from the Faculty of Engineering, University of Bologna, Bologna, Italy, in 2014.

Since 2014, he has been a Principal Researcher III with IMT-Bucharest, Voluntari, Romania. He has coauthored more than 70 articles in ISI ranked journals and conferences. His main expertise comprises the electromagnetic simulation and experimental characterization of RF/microwave/millimeter-wave/terahertz systems for wireless/energy-harvesting applications embedding carbon-based, 2-D, and nanoscale ferroelectric materials.

Dr. Aldrigo serves or has served as a reviewer for many journals and as a Co-Chair at international conferences.

M. Dragoman received the Ph.D. degree in electronics from the University "Politehnica" Bucharest, Bucharest, Romania, in 1991.

He is currently a Senior Researcher I with IMT-Bucharest, Voluntari, Romania. He has coauthored more than 250 scientific articles in ISI ranked journals and conferences, and six monographies.

Dr. Dragoman was awarded the "Gheorghe Cartianu" Prize of the Romanian Academy in 1999. He was a recipient of the Humboldt Fellowship Award and followed postdoctoral studies at Duisburg University, Germany, from 1992 to 1994.

N. Pelagalli received the Laurea degree in electronic engineering from the Polytechnic University of Marche (UnivPM), Ancona, Italy, in 2019, and he attended the Ph.D. courses at the Department of Information Engineering, UnivPM, between 2020 and 2021.

He is currently a Scientist with IHP Microelectronics, Frankfurt (Oder), Germany, with the High Data Rate Circuits Group for his Ph.D. in RF circuit design. His main interests focused on physical modeling of electronic devices based on low-dimensional materials and metamaterials-based circuits.

E. Laudadio received the Ph.D. degree (*summa cum laude*) from the Polytechnic Polytechnic University of Marche (UnivPM), Ancona, Italy, in 2016.

From 2016 to 2018, he was a Post-Doctoral Researcher with UnivPM. Since 2018, he has been a Researcher of chemical fundamentals of technologies with the Department of Materials, Environmental Sciences and Urban Planning, UnivPM. He has coauthored over 35 peer-reviewed articles, a chapter of the book "*Frontiers in Computational Chemistry*," one patent, and he presented 25 conference papers. His main research areas are *in-silico* atomistic methods based on density functional theory (DFT) and semiempirical approaches to extrapolate the constitutive relationships of nanostructured materials.

L. Zappelli (Member, IEEE) received the M.S. degree (*summa cum laude*) and the Ph.D. degree in electronic engineering from the University of Ancona, Ancona, Italy, in 1986 and 1991, respectively.

Since 1988, he has been with the Department of Information Engineering, Polytechnic University of Marche (UnivPM), Ancona, where he is currently an Assistant Professor. His research interests are microwaves, electromagnetic compatibility, phased array antennas, frequency selective surfaces, and microwave equivalent circuits.

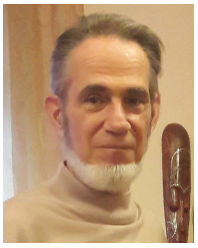

S. Iordanescu (Life Member, IEEE) received the M.S. degree from the Faculty of Electronics and Telecommunications, Polytechnic Institute of Bucharest, Bucharest, Romania, in 1972, and the Ph.D. degree in electronic engineering from the University "Politehnica" Bucharest, Bucharest, in 2000.

Since 2015, he has been a Senior Researcher with IMT-Bucharest. He has authored more than 100 scientific articles in peer-reviewed journals and conferences. His research interests include microwave SAW filter and sensor design, the characterization of dielectric and ferroelectric materials, and the design of various microwave and millimeter-wave circuits.

Dr. Iordanescu received the "Tudor Tanasescu" Romanian Academy Award (with team) in 2003.

D. Vasilache received the Ph.D. degree from the University "Politehnica" Bucharest, Bucharest, Romania, in 2011.

He is currently a Senior Researcher II with IMT-Bucharest, Voluntari, Romania. He has authored more than 150 articles (33 in ISI ranked journals). His research interests include MEMS and NEMS design, manufacturing and encapsulation, thin films deposition and patterning, masks design and manufacturing.

A. Dinescu received the M.S. and Ph.D. degrees in solid state physics from the Faculty of Physics, University of Bucharest, Bucharest, Romania, in 1993 and 2010, respectively.

From 1993 to 1997, he was with the Research Institute for Electronic Components (ICCE), Voluntari, Romania, working in the field of optoelectronics. Since 1997, he has been with IMT-Bucharest, Voluntari, where he is currently CEO and the President of the Board. He was the Head of the Nanoscale Structuring and Characterization Laboratory for 17 years and the Technical Manager of IMT for five years. He is involved in the micro and nanoscale characterization using FE-scanning electron microscope (SEM), and in structuring at the nanoscale using electron-beam lithography. He has coauthored more than 100 articles in refereed international journals and coordinated 15 national and three European research projects. His expertise also includes micro and nanofabrication, and optoelectronic measurements.

L. Pierantoni (Senior Member, IEEE) received the Laurea degree (*summa cum laude*) in electronic engineering and the Ph.D. degree in electromagnetics from the University of Ancona, Ancona, Italy, in 1988 and 1993, respectively.

From 1996 to 1999, he was a Senior Research Scientist with the Technical University of Munich, Germany, Munich, Germany. He is currently a Full Professor of electromagnetic fields with the Polytechnic University of Marche (UnivPM), Ancona. He has coauthored about 300 articles in peer-reviewed journals and conferences. His research interests are in the development of computational techniques for the multiphysics modeling of nano-to-meso-scale devices/systems, including electrodynamics, quantum mechanics, thermal effects, and spintronics.

Dr. Pierantoni has been a member of the Nanotechnology Council (NTC) AdCom, since 2012. He was a member of the International Microwave Symposium Technical Program Committee, EuMA, and Italian Institute of Nuclear Physics (INFN). He was the Co-Founder and the First Chair of the MTT-S "RF Nanotechnology" Technical Committee, the Distinguished Microwave Lecturer of the IEEE MTT-S (DML, 2012–2014), and IEEE MTT-S DML Emeritus (DML-E, 2015–2016), a Distinguished Lecturer of the IEEE Nanotechnology Council (NTC) (2015–2016). He was the Senior Editor of the IEEE TRANSACTIONS ON NANOTECHNOLOGY (TNANO), and an Associate Editor of the *Journal of Computational Electronics* (JCE) (Springer) and *Nanomaterials and Nanotechnology* (NMNT) (InTech). He is currently a Principal Investigator of several European projects.

P. Stipa received the Laurea degree in medicinal chemistry from Bologna University, Bologna, Italy, in 1983.

Then, he joined the Polytechnic University of Marche (UnivPM), Ancona, Italy, where he got a permanent position in 1988 and he is currently a Full Professor of chemistry with the Engineering Faculty and the Head of the Department of Materials, Environmental Sciences and Urban Planning. Among the founders of G.I.R.S.E (Italian Federation of EPR spectroscopists) in 1987, he spent the postdoctoral positions within the S.R.E.P (Structure et Reactivité des Especes Paramagnetiques) Group at Marseilles University, Marseilles, France. His scientific interests have always been focused on organic free radical chemistry, electron paramagnetic resonance (EPR) spectroscopy, density functional theory (DFT) calculations, and nitroxide radical synthesis and applications as antioxidants in polymers and biological systems.

D. Mencarelli (Member, IEEE) received the Laurea degree in electronic and telecommunication engineering from the Polytechnic University of Marche (UnivPM), Ancona, Italy, in 2002, and the Ph.D. degree in electronic and telecommunication engineering from UnivPM, in 2005.

Since 2014, he has been an Assistant Professor with the Department of Information Engineering, UnivPM. His research activity spans over a wide area, including coherent charge transport in low dimensional systems, photonic crystals, nanofield effect transistors, planar slot array antennas and microwave components, scanning probe microscopy, optomechanics, and phononic devices.

Dr. Mencarelli is an IEEE MTT-S Speaker Bureau, a Voting Member of the Nanotechnology Council (NTC) AdCom, a member of the Italian Institute of Nuclear Physics (INFN), a member of the MTT TC 25 Technical Committee, and an Associate Editor of *Nanomaterials and Nanotechnology* (NMNT) (InTech) and *Journal of Computational Electronics* (JCE) (Springer).